

Comprehensive Understanding of the Spatial Configurations of CeO₂ in NiO for the Electrocatalytic Oxygen Evolution Reaction: Embedded or Surface-Loaded

Wei Gao, Zhaoming Xia, Fangxian Cao, Johnny C. Ho,* Zheng Jiang,* and Yongquan Qu*

Introducing cerium (Ce) species into electrocatalysts has been recently developed as an effective approach to improve their oxygen evolution reaction (OER) performance. Importantly, the spatial distribution of Ce species in the hosts can determine the availability of Ce species either as additives or as co-catalysts, which would dictate their different contributions to the enhanced electrocatalytic performance. Herein, the comprehensive investigations on two different catalyst configurations, namely CeO₂-embedded NiO (Ce-NiO-E) and CeO₂-surface-loaded NiO (Ce-NiO-L), are performed to understand the effect of their specific spatial arrangements on OER characteristics. The Ce-NiO-E catalysts exhibit a smaller overpotential of 382 mV for 10 mA cm⁻² and a lower Tafel slope of 118.7 mV dec⁻¹, demonstrating the benefits of the embedded configuration for OER, as compared with those of Ce-NiO-L (426 mV and 131.6 mV dec⁻¹) and pure NiO (467 mV and 140.7 mV dec⁻¹), respectively. The improved OER property of Ce-NiO-E originates from embedding small-sized CeO₂ clusters into the host for the larger specific surface area, richer surface defects, higher oxygen adsorption capacity, and better optimized electronic structures of the surface active sites, as compared with Ce-NiO-L. Above findings provide a valuable guideline for and insight in designing catalysts with different spatial configurations for enhanced catalytic properties.


earth-abundant materials are considered as the two effective approaches to enable the sustainable energy conversion and storage.^[1–4] However, oxygen evolution reaction (OER), being involved in both water electrolysis with hydrogen evolution reaction as well as metal–air batteries with oxygen reduction reaction, is always suffered from the inefficient oxygen generation due to its sluggish kinetics for such a four-electron process, where significant overpotentials are required.^[5–8] In order to improve the OER catalytic property of earth-abundant, transition metal-based electrocatalysts, various strategies such as preparing ultrathin nanosheet morphologies, manufacturing heterogeneous metal/metal compound structures with controllable defects, introducing foreign elements, and tuning different constituent compositions, are adopted to provide more active sites, to facilitate more effective charge and mass transfer, and to accelerate turnover of reaction intermediates.^[9–25]

In general, doping foreign elements into catalysts can effectively modify the electronic structures and reliably introduce defects to facilitate the adsorption and conversion of active intermediates with the lower energy barrier for OER.^[7] Transition metals, especially 3d transition metals such as Fe, Mn, and Cr, are widely used as dopants to regulate the chemical states of electrocatalysts.^[26–28] Typically, incorporation of Fe atoms into NiO_x would result in the abundant catalytically active trivalent

Despite the substantial recent progress in energy harvesting, highly efficient conversion and storage of electricity generated from renewable clean energies into large-scale industrial platforms are still a crucial challenge for sustainable energy utilization. For example, the rechargeable metal–air (i.e., Al–air and Zn–air) batteries and water electrolyzer cells catalyzed by

W. Gao, Z. Xia, F. Cao, Prof. Y. Qu
Center for Applied Chemical Research
Frontier Institute of Science and Technology
and Shaanxi Key Laboratory of Energy Chemical Process Intensification
Xi'an Jiaotong University
Xi'an 710049, P. R. China
E-mail: yongquan@mail.xjtu.edu.cn

W. Gao, Prof. J. C. Ho
Department of Materials Science and Engineering
City University of Hong Kong
83 Tat Chee Avenue, Kowloon 999077, Hong Kong
E-mail: johnnyho@cityu.edu.hk

 The ORCID identification number(s) for the author(s) of this article can be found under <https://doi.org/10.1002/adfm.201706056>.

W. Gao, Prof. J. C. Ho
Shenzhen Research Institute
City University of Hong Kong
Shenzhen 518057, P. R. China

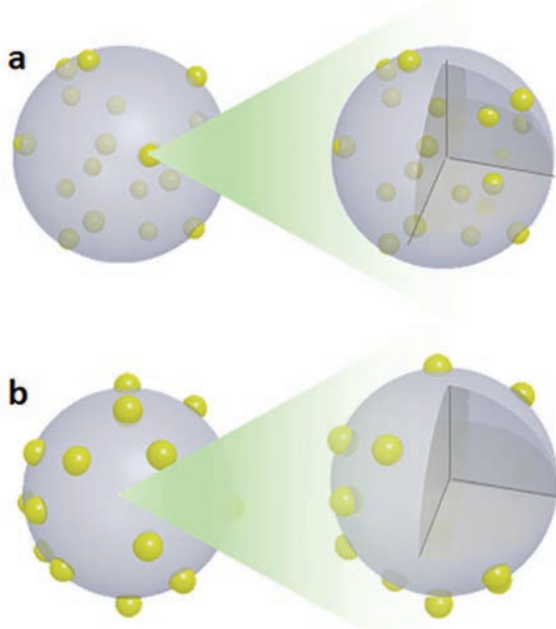
Z. Xia, Prof. Z. Jiang
Shanghai Institute of Applied Physics
Chinese Academy of Sciences
Shanghai 201204, P. R. China
E-mail: jiangzheng@sinap.ac.cn

Prof. J. C. Ho
State Key Laboratory of Millimeter Waves
City University of Hong Kong
83 Tat Chee Avenue, Kowloon 999077, Hong Kong

DOI: 10.1002/adfm.201706056

nickel and nickel vacancies to enhance OER activity.^[28] Recently, several groups reported significant improvement of the electrochemical catalytic performance on catalysts for hydrogen and oxygen generation by incorporating transitional metal-based materials with rare earth elements, namely, doping cerium into host catalysts or building heterogeneous structures between CeO₂ and active catalysts.^[29–34] Jaramillo and co-workers clarified that the geometric and electronic effects between NiO_x host and Ce dopant resulted in favorable binding energies of the OER intermediates.^[31] The promotion of FeOOH catalysts for OER by integrating CeO₂ in the heterolayered or loaded structure has been demonstrated due to the larger oxygen storage capacity of CeO₂ as well as the optimized electron interaction between CeO₂ and electrocatalysts.^[32] All the above investigations evidently reveal both of the essential strategies in introducing Ce species into the hosts and loading CeO₂ onto the surface of electrocatalysts to form heterogeneous structures, which are promising in modulating electronic structure of the surface active sites and enhancing their subsequent OER activities. However, there is still lacking of a comprehensive insight in the effect of spatial configuration on the catalytic performance of electrocatalysts whether surface-loaded Ce-based species to form heterogeneous structures or embedded Ce-based species into host materials (Scheme 1) would drive the OER process more efficiently. Understanding all these would be extremely important to develop valuable guidelines for the design of improved catalysts with appropriate spatial configuration for electrochemical reactions.

In this work, we present a comparative study on the structural and catalytic differences in NiO electrocatalysts with various spatial configurations of CeO₂ incorporation and their corresponding effects on the OER performance. In specific, two



Scheme 1. Diagrams of a) CeO₂-embedded NiO (Ce-NiO-E) and b) CeO₂-surface loaded NiO (Ce-NiO-L). The gray balls represent NiO and the yellow ones represent CeO₂ species.

CeO₂-incorporated NiO catalysts with different spatial arrangements, namely the embedded configuration of CeO₂ clusters/atoms doped NiO (Ce-NiO-E) and the surface-loaded configuration of CeO₂ nanoparticles on NiO (Ce-NiO-L), are prepared and characterized using various techniques. Interestingly, the Ce-NiO-E catalyst shows the better catalytic performance for OER with the lower overpotential of 367 mV required to reach the current density of 10 mA cm⁻², as compared with that of Ce-NiO-L (426 mV). X-ray photoelectron spectra and extended X-ray adsorption fine structure (EXAFS) analysis indicate that the low-coordinated CeO₂ clusters in Ce-NiO play an important role in creating the more catalytically active defects, promoting the oxygen adsorption capacity and facilitating the turnover of active intermediates for OER. All these comparisons elucidate explicitly the positive effect of incorporating CeO₂ with NiO, and further explain the cause of improvement in their catalytic properties by doping clusters of CeO₂, providing a novel insight of different spatially configured CeO₂ on NiO for enhanced OER catalysts.

Generally, the catalysts of NiO, Ce-NiO-E, and Ce-NiO-L were prepared through the sol-gel method followed by the high temperature annealing, as described in the Supporting Information. The embedded configuration of Ce-NiO-E and the surface-loaded configuration of Ce-NiO-L are illustrated in Scheme 1. In detail, as shown in Figure 1a, the typical transmission electron microscopy (TEM) image of NiO catalysts demonstrates their particle-like morphology with an average size of 13.6 ± 2.1 nm (Figure S1a, Supporting Information) and a specific surface area of 56 m² g⁻¹ (Figure S2, Supporting Information). The corresponding high resolution-transmission electron microscopy (HR-TEM) image in Figure 1d exhibits the atomic fringes with interplanar spacings of 0.21 and 0.24 nm, indexing to the (200) and (111) planes of the face-centered-cubic (fcc) structure of NiO, accordingly.^[28] Also, as depicted in the X-ray diffraction (XRD) pattern in Figure 2, there are four main peaks at 37.5°, 43.6°, 63.1°, and 75.5°, illustrating that the NiO catalyst consists of the fcc structure (joint committee on powder diffraction standards (JCPDS) No. 47-1049), which is perfectly consistent with the HR-TEM result. For the Ce-NiO-E catalysts, as revealed in Figure 1b, the TEM image indicates that addition of cerium preserves the similar nanoparticle morphology, but it induces a smaller particle size of 7.5 ± 1.4 nm (Figure S1b, Supporting Information) and a larger specific surface area of 90 m² g⁻¹ (Figure S2, Supporting Information), suggesting that the Ce-incorporation can prevent the formation of large NiO nanoparticles. At the same time, the corresponding XRD pattern (Figure 2) and selected area electron diffraction (SAED, Figure S3a, Supporting Information) show that there is not any apparent evidence for the existence of CeO₂ while all materials are observed with the pure phase of NiO. However, all these results cannot exclude the formation of CeO₂ due to the relatively low concentration of Ce (i.e., 5% in molar ratio) utilized during material synthesis. Evidently, further careful analysis by HR-TEM displays the existence of ultrasmall CeO₂ there, where fringes with interplanar spacings of 0.31 and 0.27 nm are corresponded to the (111) and (200) planes of the cubic fluorite structure of CeO₂,^[35] as given in Figure 1e. Moreover, there is a significant shift in the reflecting angle from 37.5° to the smaller angle of 37.3° observed in the XRD pattern (Figure 2), suggesting the expansion of cell

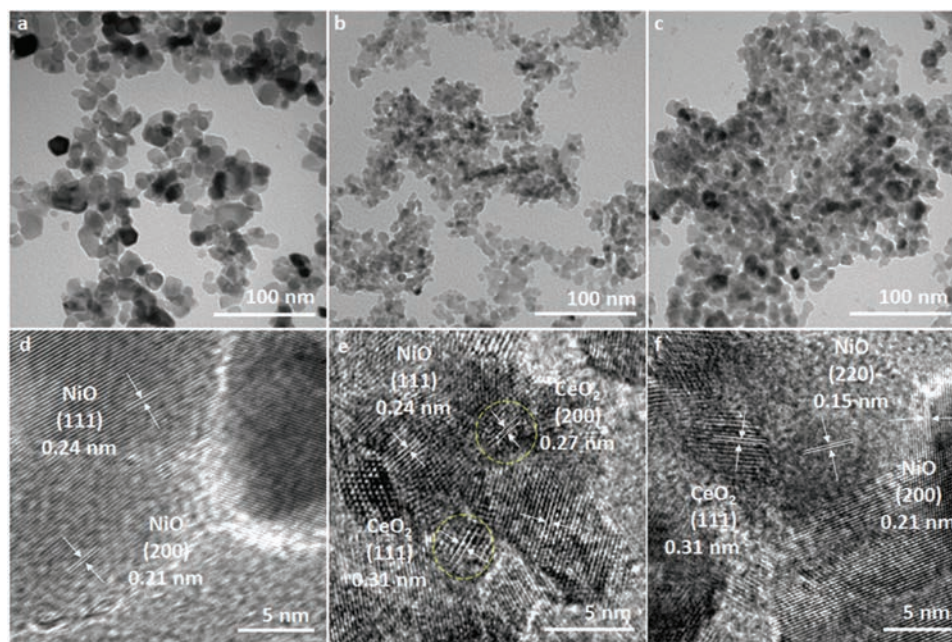


Figure 1. TEM and corresponding HR-TEM images of a,d) NiO, b,e) Ce-NiO-E, and c,f) Ce-NiO-L.

parameter from 0.4152 to 0.4172 nm as a result of introducing Ce element into the host lattice. It also indicates that some cerium species might be doped into the crystal lattice of NiO. In any case, the formation of ultrasmall CeO₂ clusters as well as the possibly cerium-doped structures does not contribute to any noticeable ceria-based XRD peaks observed in the Ce-NiO-E catalysts. Their fine structure will be further investigated in the following by combining with XAFS results in order to give a deeper insight into the structural features of catalysts induced by the addition of foreign Ce element. On the other hand, for the Ce-NiO-L catalysts, they come with an average particle size of 10.8 ± 1.8 nm (Figure S1c, Supporting Information) and a specific surface area of $65 \text{ m}^2 \text{ g}^{-1}$ (Figure S2, Supporting Information). They also consist of the fringe with interplanar spacing of 0.31 nm attributable to the (111) plane of CeO₂ and those of

0.15 and 0.21 nm corresponded to the (220) and (200) planes of NiO as clarified in the HR-TEM image (Figure 1f). Notably, the corresponding XRD pattern further confirms the existence of CeO₂ (JCPDS No. 65-0076) with apparent peaks at 28.5°, 33.1°, and 47.5° (Figure 2), being consistent with SAED pattern (Figure S3b, Supporting Information) but there is not any significant shift in the reflecting angle, excluding the doping of Ce species into NiO. As shown in Figure S4 in the Supporting Information, the energy dispersive spectrum (EDS) results as well witness the existence of Ce element in both Ce-NiO-E and Ce-NiO-L samples. Therefore, introducing Ce-based species before (cerium nitrate) and after (cerium nitrate and ammonia) obtaining the NiO precursor gels could decrease the size of NiO nanoparticles during annealing in order to form the smaller particles.

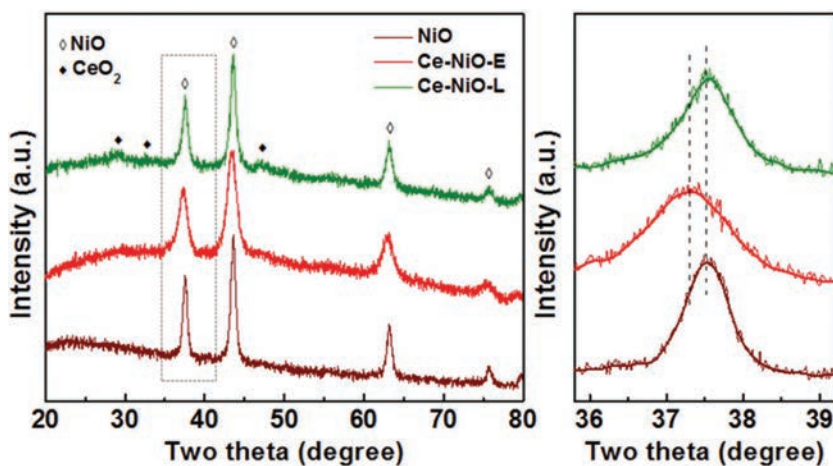


Figure 2. XRD patterns of NiO, Ce-NiO-E, and Ce-NiO-L.

To shed light on the atomic and electronic structures of the various samples, XAFS analyses are performed at Ce K-edge for Ce-NiO-E and Ce-NiO-L, where pure commercial CeO₂ is also measured as a comparison. Both Ce-NiO-E and Ce-NiO-L samples have the similar X-ray absorption near edge structures (XANES) (Figure 3a), which indicate that the Ce atoms in both Ce-NiO-E and Ce-NiO-L catalysts present the similar electronic structures as that of the commercial CeO₂ powder. Explicitly, as demonstrated in the Fourier transformed EXAFS spectra of Ce-NiO-E, Ce-NiO-L, and CeO₂ in Figure 3b, the first main peak represents the Ce-O shell for CeO₂. The reduction of Ce-O peak intensity can be ascribed to the decrease of size and the increase of disorder for Ce-NiO-E and Ce-NiO-L. The left shift of Ce-O

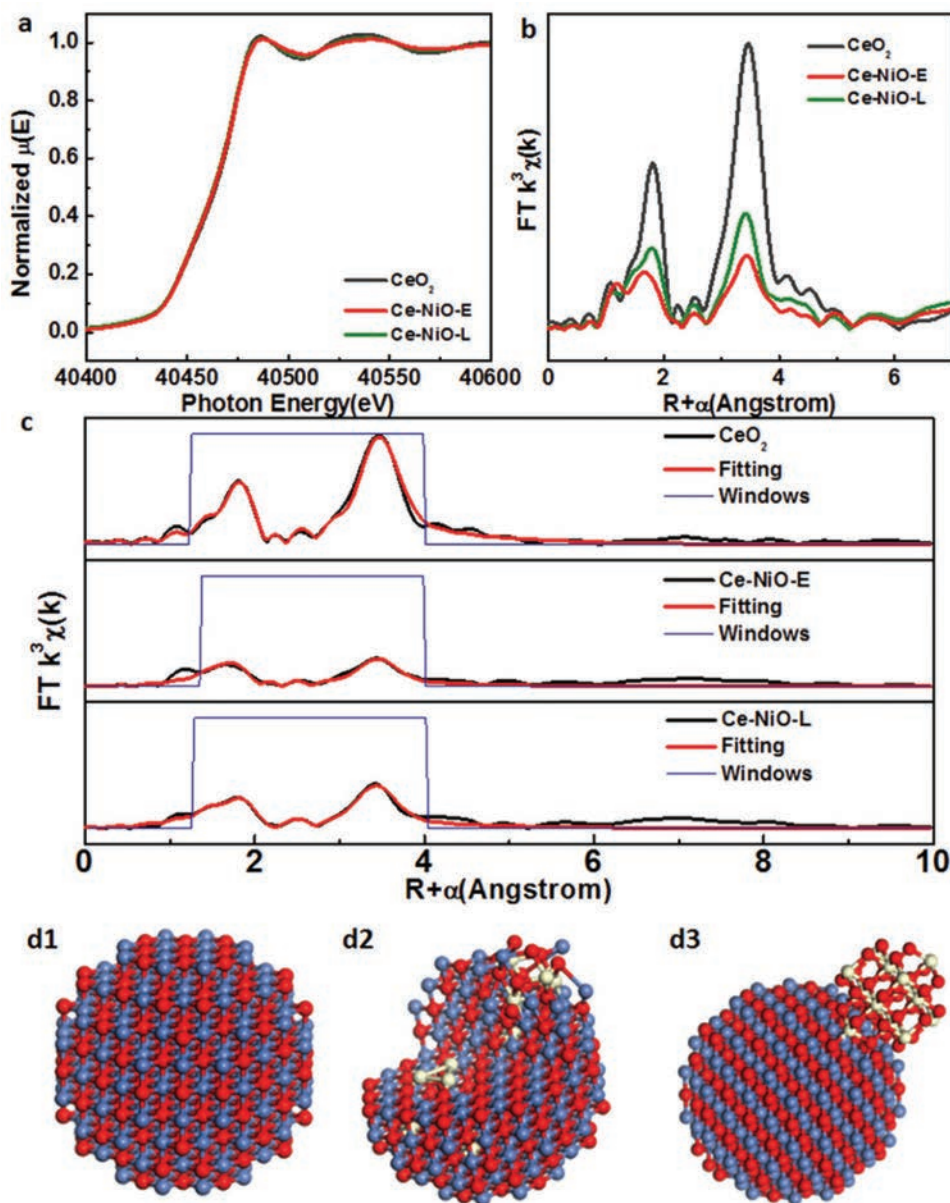


Figure 3. a) XANES results of different investigated catalysts. b) Corresponding k^3 weighted EXAFS signals in R -space and c) the fitting curves of the k^3 weighted Fourier transformed EXAFS signals in R -space of Ce-NiO-E, Ce-NiO-L, and commercial CeO₂, respectively. d) Structural models of NiO (d1), Ce-NiO-E (d2), and Ce-NiO-L (d3), red: oxygen, blue: Ni, white: Ce.

peak in Ce-NiO-E sample designates a constriction of the Ce-O bond length, which may be caused by the smaller size effect of embedded CeO₂ clusters or the incorporation (i.e., doping) of CeO₂ clusters into the NiO lattice.

Furthermore, the relationship between cluster sizes and average coordination numbers (ACNs) of Ce-Ce shell is as well shown in Figure S5 in the Supporting Information by counting the ACNs of several spherical-like CeO₂ clusters with various sizes. The experimental ACNs are determined by quantitative fitting of the EXAFS signals, as given in Figure 4 and Table 1. The Ce-Ce ACN of Ce-NiO-E sample is found to be 1.6 ± 0.9 , which demonstrates that most of the CeO₂ clusters should be composed of several atoms with the size of about 0.5 nm in this

sample, extracting from the relationship between ACNs and cluster sizes in Figure S5 in the Supporting Information. Since the CeO₂ clusters with the extremely small size of 0.5 nm are very difficult to be observed under HR-TEM, only those with the size of larger than about 1 nm are then clearly labelled in Figure 1e. The XRD pattern (Figure 2) demonstrates a distortion of NiO crystal with the extended lattice parameter in Ce-NiO-E which is caused by the CeO₂ cluster doping. This is also proved by the significant incensement of the ACN of Ce-Ni shell in Ce-NiO-E sample compared with that in Ce-NiO-L sample. The small ACN of Ce-Ni shell (0.8 ± 1.2) may be caused by the structural disorder or only few CeO₂ clusters being doped into the NiO structure while the rests are concentrated on the surface of

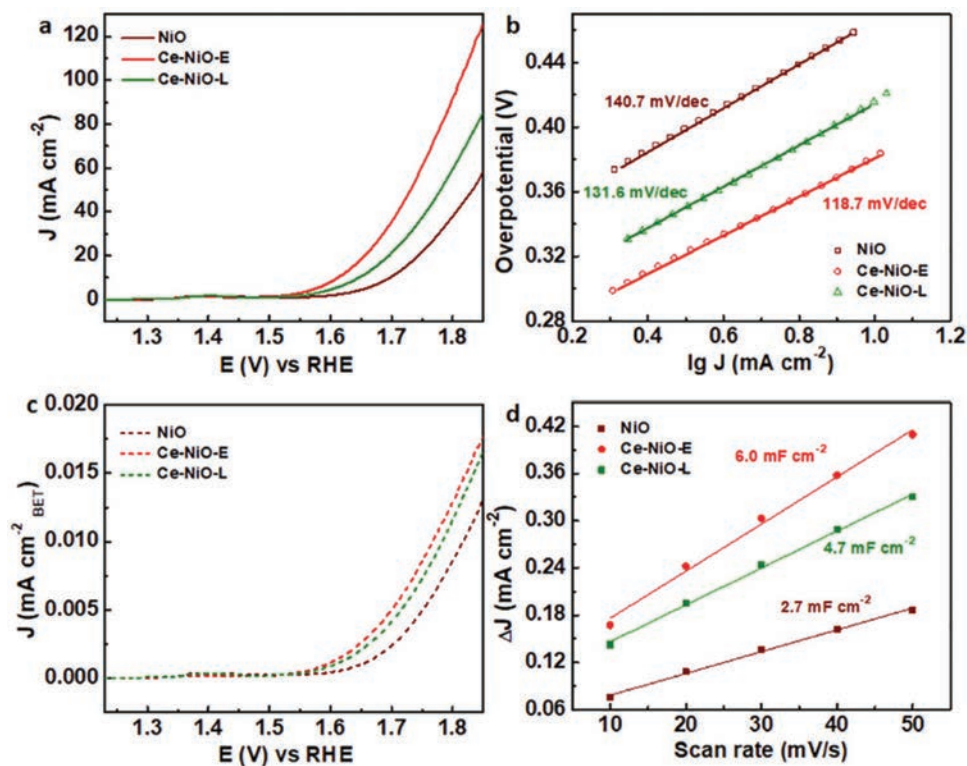


Figure 4. Electrochemical performance of NiO, Ce-NiO-E, and Ce-NiO-L in 1.0 M KOH solution. a) Polarization curves (with iR corrections), b) Tafel slopes derived from (a), c) polarization curves normalized to BET surface areas, and d) C_{dl} calculated from CV curves.

NiO. Also, for Ce-NiO-E, the bond lengths of Ce-Ni path (3.16 Å) are close to the Ni-Ni path in an NiO lattice which is also the evidence of the CeO₂-cluster-doping structure. The elongated bond length is expected since Ce has larger atomic radii compared to Ni.^[36] For Ce-NiO-L, due to the much larger ACN of Ce-Ce shell (4.4 ± 1.6), the size of CeO₂ clusters in Ce-NiO-L is postulated being larger than that of Ce-NiO-E (Figure S2, Supporting Information), in which this larger cluster size of CeO₂ can be confirmed by the corresponding HR-TEM image

in Figure 1f. As the ACN of Ce-Ni shell (<0.03, see the note in Table 1) in Ce-NiO-L is negligible as compared with the one in Ce-NiO-E, the CeO₂ clusters may be independent or favorable to form heterostructures with NiO particles for the Ce-NiO-L sample (Scheme 1). As a result, all these findings illustrate the difference of atomic structures in these two samples: doping ultrasmall CeO₂ clusters into NiO as well as surface-loading CeO₂ clusters onto NiO are realized for Ce-NiO-E to form the mosaic-like structure (Scheme 1a); while the formation of heterogeneous structure of large CeO₂ clusters on the surface of NiO is achieved for Ce-NiO-L (Scheme 1b).

Table 1. Structure parameters of Ce-NiO-E, Ce-NiO-L, and commercial CeO₂ extracted from the EXAFS fitting results.

Sample	Shell	ACN ^{a)}	σ^2 ($\times 10^{-3}$) ^{b)}	Third ($\times 10^{-3}$) ^{c)}	R^d [Å]	R -factor ^{e)}
NiO ^{f)}	Ni-O	6			2.08	
	Ni-Ni	12			2.95	
CeO ₂ ^{f)}	Ce-O	8			2.34	
	Ce-Ce	12			3.84	
Ce-NiO-E ^{g)}	Ce-O	6.0 ± 1.5	13.2 ± 1.4	0.76 ± 1.2	2.23 ± 0.06	0.019
	Ce-Ce	1.6 ± 0.9	3.1 ± 2.1		3.81 ± 0.01	
	Ce-Ni	0.8 ± 1.2	8.1 ± 2.7		3.16 ± 0.30	
Ce-NiO-L ^{h)}	Ce-O	7.3 ± 0.6	11.9 ± 2.1	1.7 ± 1.0	2.28 ± 0.06	0.012
	Ce-Ce	4.4 ± 1.6	3.6 ± 1.5		3.82 ± 0.01	

^{a)}ACN is average coordination number; ^{b)} σ^2 is Debye-Waller factor; ^{c)}Third is the third cumulants; ^{d)} R is the interatomic distance; ^{e)} R -factor is the relative error of the fitting and data; ^{f)} F_{eff} calculation of NiO (the inorganic crystal structure database (ICSD) No. 9866) and CeO₂ (ICSD No. 28753); ^{g)}Fitting results include Ce-Ni path; ^{h)}Fitting results include Ce-Ni path (ACN of Ce-Ni < 0.03) but not present.

At the same time, it is also important to investigate the surface chemical states of various electrocatalysts fabricated. As shown in the Ni 2p_{3/2} and 2p_{1/2} spectra in Figure S6 in the Supporting Information, the peaks observed at 853.8 and 871.5 eV, 855.7 and 873.5 eV, as well as 861.0 and 879.7 eV can be assigned to the Ni²⁺, Ni³⁺, and satellite peaks, respectively.^[37,38] For the O 2p spectra, peaks located at 529.4, 531.0, and 532.7 eV are ascribed to the lattice oxygen, oxygen defects and adsorbed oxygen species (e.g., hydroxides and water molecules), accordingly.^[38–41] Since both Ni³⁺ and oxygen defects play critical roles in adsorbing water molecules and forming intermediates NiOOH for OER,^[7,42] their contents can then be compared to study

the difference of NiO, Ce-NiO-E and Ce-NiO-L as electrocatalysts for OER. Importantly, there are only slight differences of Ni³⁺ and oxygen defects as observed by peak fitting. NiO comprises of the smallest surface ratios of Ni³⁺ (62%) and oxygen defects (24%), while Ce-NiO-L has the slightly higher ratios of Ni³⁺ and oxygen defects (69% and 26%, correspondingly) and Ce-NiO-E shows the highest contents of Ni³⁺ and oxygen defects (71% and 32%, correspondingly). In this case, the differences of surface chemical states here can clearly demonstrate that the two different kinds of CeO₂-NiO configured catalysts (i.e., embedded and surface-loaded) would lead to the higher Ni³⁺ contents and oxygen defects as compared with the standalone NiO, which facilitate the more efficient OER process.

After that, the OER performances of three investigated catalysts were recorded in the alkaline electrolyte (1.0 M KOH) to assess the effects of their structural differences on the catalytic properties. Though NiO has been widely studied as a catalyst for OER, its performance is still not satisfying due to the large overpotential.^[5] Polarization curves with iR corrections are exhibited in Figure 4a. To reach the current density of 10 mA cm⁻², the NiO catalyst requires a relatively large overpotential of 467 mV, while those for Ce-NiO-E and Ce-NiO-L catalysts are only 382 and 426 mV, respectively. As a control experiment, the pure CeO₂ nanoparticles are also characterized and observed to give a negligible catalytic activity for OER in 1 M KOH solution (Figure S7, Supporting Information). Derived from Figure 4a, the Tafel slope (Figure 4b) of Ce-NiO-E (118.7 mV dec⁻¹) is also much smaller than those of NiO (140.7 mV dec⁻¹) and Ce-NiO-L (131.6 mV dec⁻¹). Therefore, remarkable decreases in both overpotentials and Tafel slopes of Ce-NiO-E and Ce-NiO-L are witnessed, indicating that introducing Ce-based species can significantly improve their catalytic properties for OER. It is worth pointing that to neglect the contributions from surface areas, the specific activity normalized to the Brunauer-Emmett-Teller (BET) surface areas of various catalysts also followed the same order of Ce-NiO-E > Ce-NiO-L > NiO (Figure 4c), suggesting the great promotion of Ce involving. Moreover, as the electrochemically active specific area is proportional to the double layer capacitance (C_{dl}), the C_{dl} values of various catalysts are then usually evaluated to uncover the actual quantities of catalytic sites of electrocatalysts.^[5] Specifically, cyclic voltammetry (CV) curves (Figure S8, Supporting Information) with various scan rates for the NiO, Ce-NiO-E, and Ce-NiO-L catalysts are obtained to calculate C_{dl}. The C_{dl} value is found to be 2.7 mF cm⁻² for NiO, while those for Ce-NiO-E and Ce-NiO-L are observed to be 4.7 and 6.0 mF cm⁻², correspondingly (Figure 4c), implying that incorporating CeO₂ into the host would lead to the exposure of more active sites in order to facilitate the OER process for both Ce-NiO-E and Ce-NiO-L. All these results are perfectly consistent with the above-discussed size reduction and surface area enhancement the increased surface Ni³⁺ fractions as well as the enhanced concentrations of the interfacial oxygen defects of the NiO-based electrocatalysts with the addition of cerium species. Further investigations in the stability were also performed under a fixed overpotential of 500 mV. Both Ce-NiO-E and Ce-NiO-L catalysts exhibited the better preservation in catalytic current densities as compared with that of NiO (Figure S9, Supporting Information).

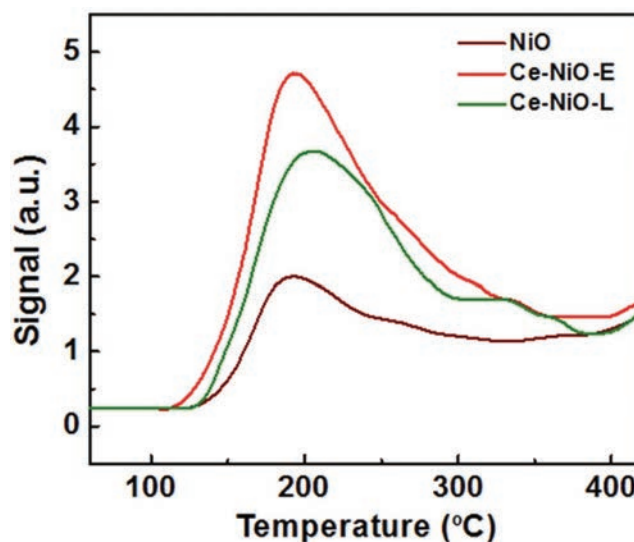


Figure 5. O₂-TPD spectra of NiO, Ce-NiO-E, and Ce-NiO-L.

Since the OER process involves a complex procedure of the adsorption of hydroxide species, formation of metal-oxygen (M-O) and metal-oxyhydroxides (M-OOH) active intermediates, and subsequent desorption of molecular oxygen, evaluating the affinity of catalysts for oxygen is also important.^[6,41] In principle, the oxygen storage capacity is previously adopted to estimate the ability of oxygen adsorption of OER catalysts, where the specific surface areas are measured under an oxygen atmosphere, as demonstrated by Li and co-workers^[32] Herein, the characteristics and difference of OER properties of various catalysts are purposely investigated from the view of oxygen adsorption and desorption capacity using an oxygen-temperature programmed desorption (O₂-TPD) method. As displayed in Figure 5, there are significant peaks at about 200 °C, which can be ascribed to the desorption of oxygen species, coming from the saturated adsorbed oxygen on the surface of catalysts during the pretreatments. For NiO, the oxygen adsorption capacity is calculated to be 15.5 μmol g⁻¹, and those for Ce-NiO-E and Ce-NiO-L are found to be 47.4 and 41.8 μmol g⁻¹, respectively. As a control, the value for CeO₂ nanoparticles is also determined to be 39.5 μmol g⁻¹ (Figure S7d, Supporting Information). Therefore, the incorporation of CeO₂ species here is concluded to promote the oxygen capacities of both Ce-NiO-E and Ce-NiO-L due to the formation of small-sized CeO₂, while Ce-NiO-E configured with the small clusters or cerium dopants as well as the larger oxygen adsorption capacity yields the best catalytic OER performance.

Based on the above findings, it is obvious that the OER performance of the NiO electrocatalysts can be substantially enhanced by incorporating Ce-based species into the host lattice with different manners. Among them, the embedded configuration of the Ce-NiO-E catalyst can deliver the much better catalytic performance with the smaller overpotential, lower Tafel slope and more active sites for OER as compared with the ones of surface-loaded configuration of the Ce-NiO-L catalysts. The differences of their catalytic properties towards OER are ascribed to their fine structures and surface chemical states of Ce-NiO-E and Ce-NiO-L. The following reasons are then summarized

to clarify their explicit differences. (1) Both embedding and surface-loading CeO₂ in NiO can effectively decrease the particle size of the host while the embedded CeO₂ can be formed in the extremely small crystal size on the order of 1 nm with the largest specific surface areas for Ce-NiO-E. (2) CeO₂ species in both Ce-NiO-E and Ce-NiO-L are known to promote the formation of M-OOH intermediate due to the high mobility of oxygen vacancies, being subsequently worked as an oxygen buffer to facilitate the evolution of oxygen.^[30,33,43] Also, the lower ACNs of Ce-O and Ce-Ce in Ce-NiO-E would suggest the smaller CeO₂ cluster size there and the more oxygen vacancies existed in the clusters as compared with those in CeO₂-NiO-L. Moreover, since the low-coordinated Ce bonding with Ni shows the good oxophilicity,^[31] the larger ACN of Ce-Ni (0.8 ± 1.2) in Ce-NiO-E can further enhance the OER property as compared to that of Ce-NiO-L with an ultrasmall ACN of Ce-Ni (<0.03). In other words, the embedded configuration of Ce-NiO-E can efficiently utilize the cerium species as the additives and consequently improve the OER activity of NiO, considering that the cerium contents in both Ce-NiO-E and Ce-NiO-L are same. (3) The modulation in electronic structures of NiO hosts examined by surface chemical states indicates that the existence of rich Ni³⁺ and oxygen defects would facilitate the adsorption/activation of water molecules and oxygen intermediates for both Ce-NiO-E and Ce-NiO-L, as compared with the pure NiO.^[42,44] Meanwhile, these rich defects could be a result of embedding the small clusters of CeO₂ into NiO in order to induce more defect formation in the host crystal of NiO, which can further benefit the efficient adsorption of intermediates. Importantly, the O₂-TPD results are consistent with previous analyses, showing the larger oxygen adsorption capacity of Ce-NiO-E as compared with that of Ce-NiO-L. Therefore, the improved catalytic property of both Ce-NiO-E and Ce-NiO-L for OER can be ascribed to the rich oxygen vacancies, modified surface chemical states and small-sized CeO₂. Among different CeO₂ configuration, the best-performed Ce-NiO-E catalyst for OER is entirely related to the doping of low-coordinated CeO₂ clusters into the NiO host, which distinguishes itself uniquely from the heterostructured Ce-NiO-L catalyst.

In summary, two different spatial configurations of the CeO₂-incorporated NiO catalysts are prepared and analyzed to evaluate their structural differences in crystallinity and electronic structures as well as these effects on their OER activity. Embedding the CeO₂ clusters into NiO exhibits the enhanced catalytic performance for OER process due to (1) the decreased catalyst particle size and the larger amount of the available surface active sites; (2) the low coordination of Ce-Ce and Ce-O to facilitate the activation and conversion of adsorbed water and intermediates; (3) the modulated electronic structures of the surface active sites with positive effects in regulating their structure properties of the NiO host. All these results also demonstrate the improved oxygen adsorption capacity of both Ce-NiO-E and Ce-NiO-L as compared with the pure NiO, which can subsequently contribute to the better catalytic activity for OER. This unique structure achieved by doping CeO₂ into NiO for Ce-NiO-E can not only promote the OER process more efficiently but also uncover a further insight in designing catalysts with different spatial configurations for the enhanced catalytic properties.

Supporting Information

Supporting Information is available from the Wiley Online Library or from the author.

Acknowledgements

W.G. and Z.X. contributed equally to this work. This work was supported by a grant from the Major State Basic Research Development Program of China (973 Program) (No. Y314052031), the National 1000-Plan program, National Natural Science Foundation of China (Grants 21401148, U1732267, and 51672229), the Science Technology and Innovation Committee of Shenzhen Municipality (Grant JCYJ20160229165240684), and the Environment and Conservation Fund of Hong Kong SAR, China (ECF 2016-85). Y.Q. was also supported by the Cyrus Tang Foundation through Tang Scholar program.

Conflict of Interest

The authors declare no conflict of interest.

Keywords

CeO₂, electrocatalysis, NiO, oxygen evolution, spatial configurations

Received: October 19, 2017

Revised: November 15, 2017

Published online: January 17, 2018

- [1] S. Chu, Y. Cui, N. Liu, *Nat. Mater.* **2017**, *16*, 16.
- [2] Z. W. Seh, J. Kibsgaard, C. F. Dickens, I. Chorkendorff, J. K. Nørskov, T. F. Jaramillo, *Science* **2017**, *355*, eaad4998.
- [3] V. R. Stamenkovic, D. Strmcnik, P. P. Lopes, N. M. Markovic, *Nat. Mater.* **2017**, *16*, 57.
- [4] I. Roger, M. A. Shipman, M. D. Symes, *Nat. Rev. Chem.* **2017**, *1*, 0003.
- [5] C. C. L. McCrory, S. Jung, J. C. Peters, T. F. Jaramillo, *J. Am. Chem. Soc.* **2013**, *135*, 16977.
- [6] N.-T. Suen, S.-F. Hung, Q. Quan, N. Zhang, Y.-J. Xu, H. M. Chen, *Chem. Soc. Rev.* **2017**, *46*, 337.
- [7] L. Han, S. J. Dong, E. K. Wang, *Adv. Mater.* **2016**, *28*, 9266.
- [8] T. Reier, H. N. Nong, D. Teschner, R. Schlögl, P. Strasser, *Adv. Energy Mater.* **2016**, *7*, 1601275.
- [9] X. M. Zhou, Z. M. Xia, Z. Y. Zhang, Y. Y. Ma, Y. Q. Qu, *J. Mater. Chem. A* **2014**, *2*, 11799.
- [10] S. L. Zhao, Y. Wang, J. C. Dong, C.-T. He, H. J. Yin, P. F. An, K. Zhao, X. F. Zhang, C. Gao, L. J. Zhang, J. W. Lv, J. X. Wang, J. Q. Zhang, A. M. Khattak, N. A. Khan, Z. X. Wei, J. Zhang, S. Q. Liu, H. J. Zhao, Z. Y. Tang, *Nat. Energy* **2016**, *1*, 16184.
- [11] Y. W. Liu, H. Cheng, M. J. Lyu, S. J. Fan, Q. H. Liu, W. S. Zhang, Y. D. Zhi, C. M. Wang, C. Xiao, S. Q. Wei, B. J. Ye, Y. Xie, *J. Am. Chem. Soc.* **2014**, *136*, 15670.
- [12] Z. Liu, Z. Zhao, Y. Wang, S. Dou, D. Yan, D. Liu, Z. Xia, S. Wang, *Adv. Mater.* **2017**, *29*, 1606207.
- [13] H. Xu, J.-X. Feng, Y.-X. Tong, G.-R. Li, *ACS Catal.* **2017**, *7*, 986.
- [14] B. Zhang, X. L. Zheng, O. Voznyy, R. Comin, M. Bajdich, M. García-Melchor, L. L. Han, J. X. Xu, M. Liu, L. R. Zheng, F. P. G. De Arquer, C. T. Dinh, F. J. Fan, M. J. Yuan, E. Yassitepe, N. Chen, T. Regier, P. F. Liu, Y. H. Li, P. D. Luna, A. Janmohamed,

- H. L. L. Xin, H. G. Yang, A. Vojvodic, E. H. Sargent, *Science* **2016**, 333.
- [15] S. Dou, C.-L. Dong, Z. Hu, Y.-C. Huang, J.-I. Chen, L. Tao, D. Yan, D. Chen, S. Shen, S. Chou, S. Wang, *Adv. Funct. Mater.* **2017**, 27, 1702546.
- [16] X. Zhao, H. T. Zhang, Y. Yan, J. H. Cao, X. Q. Li, S. M. Zhou, Z. M. Peng, J. Zeng, *Angew. Chem., Int. Ed.* **2017**, 56, 328.
- [17] Z. Xiao, Y. Wang, Y.-C. Huang, Z. Wei, C.-L. Dong, J. Ma, S. Shen, Y. Li, S. Wang, *Energy Environ. Sci.* **2017**, 10, 2563.
- [18] X. Liu, Z. Chang, L. Luo, T. Xu, X. Lei, J. Liu, X. Sun, *Chem. Mater.* **2014**, 26, 1889.
- [19] R. Liu, Y. Wang, D. Liu, Y. Zou, S. Wang, *Adv. Mater.* **2017**, 29, 1701546.
- [20] X.-F. Lu, P.-Q. Liao, J.-W. Wang, J.-X. Wu, X.-W. Chen, C.-T. He, J.-P. Zhang, G.-R. Li, X.-M. Chen, *J. Am. Chem. Soc.* **2016**, 138, 8336.
- [21] D. Yan, Y. Li, J. Huo, R. Chen, L. Dai, S. Wang, *Adv. Mater.* **2017**, 29, 1606459.
- [22] L. Xu, Q. Jiang, Z. Xiao, X. Li, J. Huo, S. Wang, L. Dai, *Angew. Chem.* **2016**, 128, 5363.
- [23] Y. Wang, Y. Zhang, Z. Liu, C. Xie, S. Feng, D. Liu, M. Shao, S. Wang, *Angew. Chem., Int. Ed.* **2017**, 56, 5867.
- [24] X.-F. Lu, L.-F. Gu, J.-W. Wang, J.-X. Wu, P.-Q. Liao, G.-R. Li, *Adv. Mater.* **2017**, 29, 1604437.
- [25] J.-X. Feng, H. Xu, Y.-T. Dong, S.-H. Ye, Y.-X. Tong, G.-R. Li, *Angew. Chem., Int. Ed.* **2016**, 55, 3694.
- [26] C.-C. Lin, C. C. L. McCrory, *ACS Catal.* **2017**, 7, 443.
- [27] T. Tang, W.-J. Jiang, S. Niu, N. Liu, H. Luo, Y.-Y. Chen, S.-F. Jin, F. Gao, L.-J. Wan, J.-S. Hu, *J. Am. Chem. Soc.* **2017**, 139, 8320.
- [28] G. Wu, W. X. Chen, X. S. Zheng, D. P. He, Y. Q. Luo, X. Q. Wang, J. Yang, Y. E. Wu, W. S. Yan, Z. B. Zhuang, X. Hong, Y. D. Li, *Nano Energy* **2017**, 38, 167.
- [29] J. A. Haber, Y. Cai, S. Jung, C. X. Xiang, S. Mitrovic, J. Jin, A. T. Bell, J. M. Gregoire, *Energy Environ. Sci.* **2014**, 7, 682.
- [30] Y.-R. Zheng, M.-R. Gao, Q. Gao, H.-H. Li, J. Xu, Z.-Y. Wu, S.-H. Yu, *Small* **2015**, 11, 182.
- [31] J. W. D. Ng, M. García-Melchor, M. Bajdich, P. Chakthranont, C. Kirk, A. Vojvodic, T. F. Jaramillo, *Nat. Energy* **2016**, 1, 16053.
- [32] J.-X. Feng, S.-H. Ye, H. Xu, Y.-X. Tong, G.-R. Li, *Adv. Mater.* **2016**, 28, 4698.
- [33] Z. Q. Liu, N. Li, H. Y. Zhao, Y. Zhang, Y. H. Huang, Z. Y. Yin, Y. P. Du, *Chem. Sci.* **2017**, 8, 3211.
- [34] W. Gao, M. Yan, H.-Y. Cheung, Z. M. Xia, X. M. Zhou, Y. B. Qin, C.-Y. Wong, J. C. Ho, C.-R. Chang, Y. Q. Qu, *Nano Energy* **2017**, 38, 290.
- [35] J. Li, Z. Y. Zhang, Z. M. Tian, X. M. Zhou, Z. P. Zheng, Y. Y. Ma, Y. Q. Qu, *J. Mater. Chem. A* **2014**, 2, 16459.
- [36] L. L. Lu, Y. Y. Jia, X.-X. Ye, M. Luo, F. Song, Y. Y. Huang, X. T. Zhou, Z. J. Li, Z. Jiang, *Corros. Sci.* **2016**, 108, 169.
- [37] L.-L. Wu, Z. Wang, Y. Long, J. Li, Y. Liu, O.-S. Wang, X. Wang, S.-Y. Song, X. G. Liu, H.-J. Zhang, *Small* **2017**, 13, 1604270.
- [38] W. X. Guo, W. W. Sun, Y. Wang, *ACS Nano* **2015**, 9, 11462.
- [39] T. V. Thi, A. K. Rai, J. Gim, J. Kim, *J. Power Sources* **2015**, 292, 23.
- [40] B. P. Payne, M. C. Biesigner, N. S. McIntyre, *J. Electron Spectrosc. Relat. Phenom.* **2012**, 185, 159.
- [41] J. Bao, X. D. Zhang, B. Fan, J. J. Zhang, M. Zhou, W. L. Yang, X. Hu, H. Wang, B. C. Pan, Y. Xie, *Angew. Chem.* **2015**, 127, 7507.
- [42] K. Fominykh, J. M. Feckl, J. Sicklinger, M. D. Döblinger, S. Böcklein, J. Ziegler, L. Peter, J. Rathousky, E.-W. Scheidt, T. Bein, D. Fattakhova-Rohlfing, *Adv. Funct. Mater.* **2014**, 24, 3123.
- [43] K. Liu, X. B. Huang, H. Y. Wang, F. Z. Li, Y. G. Tang, J. S. Li, M. H. Shao, *ACS Appl. Mater. Interfaces* **2016**, 8, 34422.
- [44] S. Anantharaj, S. R. Ede, K. Sakthikumar, K. Karthick, S. Mishra, S. Kundu, *ACS Catal.* **2016**, 6, 8069.